frontiers | Frontiers in Network Physiology

TYPE Original Research
PUBLISHED 24 June 2024
DOI 10.3389/fnetp.2024.1393397

OPEN ACCESS

EDITED BY
Quan Zhang,
University of Oxford, United Kingdom

REVIEWED BY
Andrei I Tarasov,
Ulster University, United Kingdom
Rene Markovič,
University of Maribor, Slovenia
Huixia Ren,
Peking University, China
Jan Zmazek,
University of Maribor, Slovenia

*CORRESPONDENCE
Vira Kravets,
vkravets@ucsd.edu

RECEIVED 29 February 2024
ACCEPTED 21 May 2024
PUBLISHED 24 June 2024

CITATION
Balasenthilkumaran NV, Whitesell JC, Pyle L, Friedman RS and Kravets V (2024), Network approach reveals preferential T-cell and macrophage association with α-linked β-cells in early stage of insulitis in NOD mice. *Front. Netw. Physiol.* 4:1393397. doi: 10.3389/fnetp.2024.1393397

Network approach reveals preferential T-cell and macrophage association with α-linked β-cells in early stage of insulitis in NOD mice

Nirmala V. Balasenthilkumaran[1], Jennifer C. Whitesell[2], Laura Pyle[3], Rachel S. Friedman[2] and Vira Kravets[1,4]*

[1]Department of Bioengineering, Jacobs School of Engineering, University of California San Diego, San Diego, CA, United States, [2]Department of Immunology and Microbiology, School of Medicine, Barbara Davis Center for Diabetes, University of Colorado Anschutz Medical Campus, Aurora, CO, United States, [3]Department of Pediatrics, University of Colorado School of Medicine, Department of Biostatistics and Informatics, Colorado School of Public Health, Aurora, CO, United States, [4]Department of Pediatrics, School of Medicine, University of California San Diego, San Diego, CA, United States

One of the challenges in studying islet inflammation–insulitis–is that it is a transient phenomenon. Traditional reporting of the insulitis progression is based on cumulative, donor-averaged values of leucocyte density in the vicinity of pancreatic islets, that hinder intra- and inter-islet heterogeneity of disease progression. Here, we aimed to understand why insulitis is non-uniform, often with peri-insulitis lesions formed on one side of an islet. To achieve this, we demonstrated the applicability of network theory in detangling intra-islet multi-cellular interactions during insulitis. Specifically, we asked the question "What is unique about regions of the islet that interact with immune cells first". This study utilized the non-obese diabetic mouse model of type one diabetes and examined the interplay among α-, β-, T-cells, myeloid cells, and macrophages in pancreatic islets during the progression of insulitis. Disease evolution was tracked based on the T/β cell ratio in individual islets. In the early stage, we found that immune cells are preferentially interacting with α-cell-rich regions of an islet. At the islet periphery α-linked β-cells were found to be targeted significantly more compared to those without α-cell neighbors. Additionally, network analysis revealed increased T-myeloid, and T-macrophage interactions with all β-cells.

KEYWORDS

insulitis, network, alpha cells, diabetes, first responder beta cells, network physiology

1 Introduction

Tracking evolution of islet inflammation: Type 1 diabetes mellitus (T1D) is an autoimmune disorder, characterized by a progressive loss of pancreatic β-cells, a decrease in insulin secretion, and an increase in blood glucose levels (Coppieters et al., 2012). T1D islet inflammation, known as insulitis, is associated with β-cell dysfunction and death, has a transient nature in that it clears following complete β-cell loss in an islet, and is usually observed within 1 year of diabetes onset in humans. Additionally, our work shows that the pathogenic behavior of islet-infiltrating T-cells is dependent on the severity of insulitis (Friedman et al., 2014; Lindsay et al., 2015). Previous studies indicate a

heterogenous pattern of CD8 T-cell infiltration in human pancreatic islets during the early stages of T1D (Coppieters et al., 2012; Rodriguez-Calvo et al., 2015; Damond et al., 2019). Here we utilized the non-obese diabetic (NOD) mouse model - one of the most widely studied diabetic mouse models, with features similar to human T1D (Kikutani and Makino, 1992; Anderson and Bluestone, 2005; Chen et al., 2020). We applied an islet sorting algorithm based on the T/β cell ratio in individual islets to account for differences in the amount of infiltration in various islets, which allows to assign a disease stage to each islet. Islet-wise classification has been previously performed to indicate the stage of insulitis (Carrero et al., 2013; Katsarou et al., 2017; Damond et al., 2019).

Detangling multi-cellular interactions to understand non-uniform inflammation of an islet: In an islet, peri-insulitis is often observed on one side of an islet (Morgan et al., 2014). We, therefore, asked a question: What is unique about the regions of an islet that are affected by peri-insulitis? With this in mind, we then aimed to detangle multi-cellular immune-endocrine interactions by applying network theory analysis–a mathematical method used for studying the relationships between a set of nodes (cells in our case). Network analysis has been successfully applied to analyze protein-protein interactions, gene regulation, and metabolic pathways at the cellular level (Jeong et al., 2000; Barabási and Oltvai, 2004; Schlitt and Brazma, 2007). It has also been used to better understand neuronal architecture and human disease (Bullmore and Sporns, 2009; Barabási et al., 2011). However, more recently it has been applied to conduct *functional* analysis based on the coordination of calcium dynamics in endocrine pancreatic islets (Stožer et al., 2013; Johnston et al., 2016; Kravets et al., 2022; Stožer et al., 2022). *Spatial* network analysis is based on cell-cell proximity and has been previously used to study the organization and interactions of α-, β-, and δ-cells in an islet (Hoang et al., 2014; Gosak et al., 2022). Immune cells interact with islet cells through contact-dependent mechanisms, enabling the quantitative analysis of these interactions by assessing the proximity between these cell types (Cnop et al., 2005; Burrack et al., 2017). Specifically, T-cells interact with β-cells via well-defined ligand-based interactions: the T-cell receptor (TCR) on $CD8^+$ T-cells recognizes antigens presented by HLA class I molecules on β-cells, and the Fas ligand on $CD8^+$ T-cells binds to the Fas receptor on β-cells, providing a secondary interaction pathway (Daniels and Jameson, 2000; Dudek et al., 2006; Mariuzza et al., 2020). Additionally, myeloid cells and macrophages interact with β-cells by phagocytosing intact or apoptotic β-cells and their debris, followed by antigen presentation and upregulation of MHC class I and II molecules, recognized by $CD8^+$ and $CD4^+$ T-cells' TCRs, facilitating further contact-based interactions (Friedl and Gunzer, 2001; Vomund et al., 2015). Islet cells also exhibit paracrine signaling, intensified by closer proximity among cells, which is pivotal in the islet's functional dynamics (Caicedo, 2013). Recently, spatial network analysis was adopted to show that α-cells are not randomly organized in C57BL/6 mouse islets (Tran Thi Nhu et al., 2017). The number of direct α–α connections was shown to be greater in the experimentally derived network than in a network of randomly connected islet cells (Tran Thi Nhu et al., 2017). In the present study, we utilized spatial networks, where links were assigned based on the cell-cell proximity. To assess whether our observed spatial interactions are merely due to chance, we created random networks by assigning random positions to immune cells, while preserving their empirically derived average distances to the neighboring endocrine cells, and leaving the positions of the endocrine cells intact. We then tracked the network evolution over the disease progression pseudo time, based on the T/β spectrum, described above.

Pancreatic tissue slices from non-diabetic NOD mice of ages [16–23 weeks] were used to develop a workflow to quantify heterotypic interactions between α-cells, different β-cell subpopulations (α-linked and non-α-linked), and various immune cell types. We sought to investigate if β-cells closer to α-cells, interact more with immune cells during T1D, as the destruction of these cells could explain the loss in the first phase of insulin response observed in individuals with pre-diabetes.

2 Materials and methods

2.1 Animal care

NOD/ShiLtJ mice (001976) were obtained from The Jackson Laboratory and bred in-house. All animal procedures were approved by the Institutional Animal Care and Use Committee at the University of Colorado Anschutz Medical Campus.

2.2 Immunofluorescence and imaging of mouse pancreas

WT NOD females were 16–23 weeks of age, with blood glucose readings below 250 mg/dL. The whole pancreas was excised and fixed in formalin (VWR) for 24 h. After fixation, samples were stored in 70% ethanol until paraffin embedding. 4 μm sections were cut. Embedding and sectioning were performed by the University of Colorado Anschutz histology core. Samples were stained using a Leica Autostainer and imaged using whole tissue scanning on the Akoya Polaris Imaging System.

In collaboration with the Human Immune Monitoring Shared Resource (HIMSR) at the University of Colorado School of Medicine, we performed 7 color multispectral imaging using the Akoya Biosciences Vectra Polaris instrument. Six markers were utilized, including insulin (β-cells), glucagon (α-cells), CD11c (for myeloid cells, including dendritic cells, monocytes, and macrophages), CD3 (for T cells), F4/80 (for macrophages). Myeloid cells include any cell type that develops/differentiates from a common myeloid progenitor. Myeloid cells include two major categories: 1) mononuclear phagocytes and 2) granulocytes. This experiment stains for mononuclear phagocytes, which are comprised of 3 myeloid subsets: Monocytes, Macrophages, and Dendritic Cells. This experiment does not stain for granulocytes (Neutrophils, Eosinophils, Basophils, Mast cells), which are also myeloid subsets.

The slides were stained on the Leica Bond RX autostainer according to standard protocols provided by Leica and Akoya Biosciences. Briefly, the slides were deparaffinized, heat treated in antigen retrieval buffer, blocked, and incubated with primary antibody, followed by horseradish peroxidase (HRP)-conjugated secondary antibody polymer (Akoya), and HRP-reactive OPAL fluorescent reagents (Akoya) that use TSA chemistry to deposit dyes on the tissue immediately surrounding each HRP molecule. To prevent further deposition of fluorescent dyes in

TABLE 1 Summary of immunofluorescence staining reagents used in our study.

Target	Supplier	Catalog number (S)	Clone	OPAL Dye	Antigen retrieval
Ms CD3	Cell signaling technology	999,440	D4V8L	570	pH9
Ms Insulin	Cell signaling technology	4,590	Polyclonal	480	pH6
Ms CD11c	Cell signaling technology	97,585	D1V9Y	520	pH6
Ms Glucagon	Cell signaling technology	2,760	Polyclonal	620	pH6
Ms F4/80	Cell signaling technology	30,325	D4C8V	780	pH6

subsequent staining steps, the slides were stripped in between each stain with heat treatment in antigen retrieval buffer (Akoya). Whole slide scans were collected by widefield fluorescent imaging using a 20x/NA = 0.75 objective and a pixel size of 0.5 μm/px. inForm software was used to unmix the 7 color images and subtract autofluorescence. Table 1 describes the reagents, including antibodies and their specific details such as suppliers, catalog numbers, clones, OPAL dye wavelengths, and antigen retrieval conditions used in our immunofluorescence staining protocols.

2.3 Image analysis

All image analysis was primarily done in ImageJ (FIJI) using pre-existing plugins (Schindelin et al., 2012). Akoya Polaris whole slide viewer software (Akoya Biosciences and The Spatial Biology Company, Marlborough, United States of America), and Imaris (Bitplane, Zurich, Switzerland) were used for nuclei segmentation.

2.4 Pre-processing

A smaller section, corresponding to a single islet was first manually segmented from a whole slide image, that represented the entire pancreatic slice. To account for bleed through of signal from the insulin channel into the other channels, we subtracted the regions corresponding to β-cells detected in the insulin channel from the CD11c, CD3, and F4/80 channels. As the β-cells in the pancreas are not anticipated to exhibit positive staining for the immune cell markers, we reasoned that the observed immune cell marker signal in regions of β-cells is likely due to bleed through. As expected, we observed the highest amount of bleed-through between the spectrally neighboring insulin and CD11c channels (see also Colocalization Analysis section below). Supplementary Figure S3C,D represent the CD11c channel of an islet before and after bleed through correction. The outline of the islet was manually sketched around the α- and β-cells. The islet selection was then enlarged by 60 μm to encompass the immune cells present in the periphery of the islet. The selection was then replicated in the images corresponding to other channels. Finally, the images were filtered by a median filter of radius 2 pixels to minimize background noise.

2.5 Nuclei segmentation

For every islet, the channel corresponding to its DAPI staining was overlaid with another channel of interest in the Akoya Polaris whole slide viewer software to visualize the locations of the nuclei of the corresponding cell type. The image corresponding to that channel was loaded in Imaris. Spots were manually added in Imaris by referring to the overlaid image in the whole slide viewer software to represent the nuclei. The positions of the nuclei (as X and Y coordinates) were then exported from Imaris for further analysis.

2.6 Colocalization Analysis

To test the colocalization of signal from different channels in the same cell, we calculated the Manders coefficients using the previously reported colocalization threshold plugin in ImageJ (Manders et al., 1993; Costes et al., 2004). The Manders colocalization coefficients between two channels - 1 and 2 of 'n' pixels of intensities 'P1' and 'P2' can be approximated as shown in equations (1) and (2) (Manders et al., 1993; Costes et al., 2004):

$$M_1 = \frac{\sum_{P1>T}^{i=1:n} P1_i}{\sum_{i=1:n} P1_i} \quad (1)$$

$$M_2 = \frac{\sum_{P2>aT+b}^{i=1:n} P2_i}{\sum_{i=1:n} P2_i} \quad (2)$$

Here, 'T' is an intensity threshold for channel 1 that was automatically determined by the plugin's iterative algorithm, and 'aT + b' is its corresponding intensity in channel 2 (constants 'a' and 'b' were determined by fitting the intensities of channel 1 with channel 2). Threshold 'T' was first initialized with a high value of intensity. Pearson's correlation coefficient was computed between the channels for the pixels whose intensities are below threshold 'T' in channel 1 and 'aT + b' in channel 2. Threshold 'T' was decreased until this correlation coefficient was zero. Results are shown in Supplementary Figure S1.

2.7 Ranking of insulitis progression

Progression of insulitis was ranked by computing the ratio of T-cells to β-cells (insulitis degree), as shown in Eq. 3. For every islet, the number of T-cells and β-cells that were inside the islet plus within 60 μm of the islet rim were considered, and their ratio was computed using Eq. 3. We then categorized the islets as early-, intermediate-, and late-stage islets on a spectrum. We categorized the first 44 islets in this spectrum with T/β cell ratios between 0 and 0.51 as early-stage insulitis, the next 46 islets with T/β cell ratios between 0.51 and 1.25 as

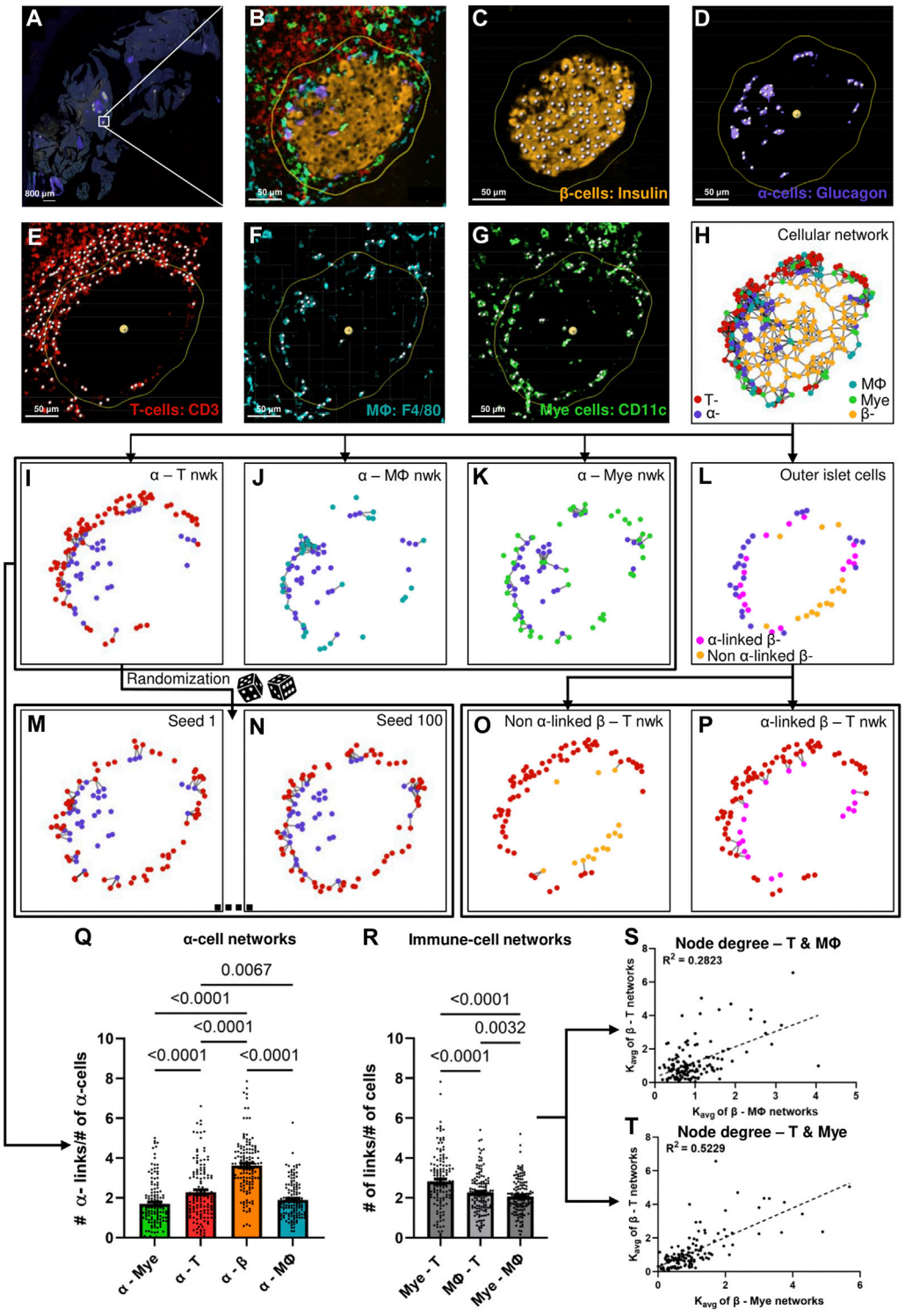

FIGURE 1
(A) Representative whole slide image of a pancreatic slice, white box represents the islet of interest. **(B)** Representative islet cropped from the whole slide image shown in **(A)** **(C)** β-cell nuclei segmented from the insulin signal extracted from the islet shown in **(B)**. **(D)** α-cell nuclei segmented from the glucagon signal extracted from the islet shown in **(B)**. **(E)** T-cell nuclei segmented from the CD3 signal extracted from the islet shown in **(B)**. **(F)** Macrophage (Mϕ) nuclei segmented from the F4/80 signal extracted from the islet shown in **(B)**. **(G)** Myeloid (Mye) cell nuclei segmented from the CD11c signal extracted from the islet shown in **(B)**. Yellow outlines in **(B–G)** represents distance of 20 µm from the islet rim, white spots in **(C–G)** represents nuclei. **(H)** Representative network of the islet shown in **(B)** created using the cellular positions obtained in **(C–G)**. **(I)–(K)** represent α-T, α-macrophage, and α-myeloid cell networks of the islet shown in **(B)** created using cellular positions obtained in **(C–G)**. **(L)** Representation of the outer layer of islet cells of the islet shown in **(B)** created from the network shown in **(H)**. **(M)** and **(N)** represent random networks obtained by randomizing the positions of T-cells in the network shown in **(I)**. **(O)** and **(P)** represent the α-linked β-T and non-α-linked β-T networks created using the outer layer of islet cells obtained in **(L)** and the positions of T-cells obtained in **(E)**. **(Q)** Comparison of K_{avg} of different α-cell networks using network analysis (n = 134 islets
(*Continued*)

FIGURE 1 (Continued)
from 11 mice) (RM one way ANOVA with Geisser-Greenhouse correction and Tukey's multiple comparisons tests were used for statistical analysis) **(R)** Comparison of K_{avg} of different immune cell networks using network analysis (n = 134 islets from 11 mice) (RM one-way ANOVA with Geisser-Greenhouse correction and Tukey's multiple comparisons tests were used for statistical analysis). **(S)** Relationship between the node degrees of β-macrophage and β-T networks obtained using network analysis (n = 134 islets from 11 mice) (Simple linear regression was used for statistical analysis). **(T)** Relationship between the node degrees of β-myeloid and β-T networks obtained using network analysis (n = 134 islets from 11 mice) (Simple linear regression was used for statistical analysis). See Materials and Methods for detailed description on pre-processing, segmentation, network analysis, outer-islet cell analysis, and randomization.

intermediate-stage insulitis, and the last 44 islets with T/β cell ratios greater than 1.25 as late-stage insulitis.

$$\textit{Insulitis degree} = \frac{\#\ of\ T-cells}{\#\ of\ \beta-cells} \tag{3}$$

As detailed in the results, we observed heterogeneity in the amount of peri-insulitis and infiltration of different islets in the same mouse (see Supplementary Figure S4F for mouse-by-mouse distribution of insulitis degrees). Mouse #5 had 14 islets with T-cells to β-cells ratios ranging from 0.065 to 5.692. Six of these islets were classified as early-stage insulitis, 3 islets were classified as intermediate-stage insulitis, and 5 islets were classified as late-stage insulitis. Similarly, mouse #2 had 1 early-stage islet, 4 intermediate-stage islets, and 6 late-stage islets with ratios ranging from 0.257 to 7.800. Different stages of islet inflammation are shown in Figure 2A.

2.8 Cellular network construction

Cellular interactions were modeled as a graph, where cells were considered nodes, and links were assigned between the nodes based on their proximity to each other. The islet mask was enlarged by 20 μm, and all immune cells located within this mask were considered to be in the network. Since, we referred to the position of a cell using the position of its nucleus, all distances specified in this paper correspond to center-to-center distances between cells. The distance for cells to be considered interacting varied between 15 μm, 20 μm, and 25 μm (results for each option were reported separately). Additionally, links were constructed only between cells of differing cell types, as we are interested only in the heterotypic interactions between cells. Two-cell networks were constructed between α- and β-cells, α- and T-cells, α-cells and macrophages, α- and myeloid cells, and three-cell networks were constructed between [α-, β-, T-] cells, [α-, β-, macrophage] cells and [α-, β-, myeloid] cells for further analysis.

2.9 Network analysis

All network construction and network analysis algorithms were done in MATLAB (MathWorks, Natick, United States of America) using custom scripts. The amount of cellular interactions between two cell types was quantified by computing the average number of connections or links (K_{avg}) of a particular cell type in a two-cell network. Average links refers to the mean number of connections a cell has in the network. It can be mathematically expressed as shown in equations (4) and (5). Three-cell networks were used to quantify the interactions between T-cells/macrophages/myeloid cells and α-linked β-cells vs. non- α-linked β-cells. Specifically, β-cells linked to α-cells were first identified, and then two-cell networks were created between α-linked β-cells and one immune cell type. The same was done for the non-α-linked β-cells and one immune cell type.

$$K_{avg} = \frac{\#\ of\ links\ of\ each\ cell}{\#\ of\ cells} \tag{4}$$

$$K_{avg}^{cell\ type\ 1} = \frac{\#\ of\ links\ of\ each\ cell\ of\ type\ 1}{\#\ of\ cells\ of\ type\ 1} \tag{5}$$

2.10 Randomizing procedure

This randomization procedure was used to create random heterotypic networks for the assessment of the likelihood of our observations being due to chance. The positions of the α- and β-cells were fixed, and the immune cells were randomly distributed around the islet rim. The immune cells were classified into two categories–inside the islet and outside the islet, based on their location with respect to the islet rim. First, the immune cells outside the islet were considered, and the distance of each cell to the islet rim was computed. A normal distribution of 1,000 distances was created using the mean and standard deviation of these experimentally determined distances. Next, the algorithm randomly replaced each immune cell's distance with a random distance from the above-mentioned normal distribution. In this manner, each immune cell was randomly repositioned within the islet periphery, while the average distance of all immune cells to the islet rim almost remained the same. The same procedure was adopted to randomize the positions of immune cells inside the islet. The randomization process was repeated 100 times. Each time (each seed), the set of distances randomly picked from the normal distribution, and the positions randomly assigned to cells, were varied.

2.11 Outer islet cell analysis

In order to account for 1) α-cells being predominantly located at the islet periphery, and 2) islet cells at the islet periphery having more opportunity to interact with the immune peri-insulitis, compared to cells located in the islet core, we performed an analysis of the *outer cell layer*, as described further. Only cells at a distance of 20 μm from the islet rim (20 μm inside the islet and 20 μm outside the islet) were considered. Three-cell networks were created using i) α-, ii) β-cells in the outer layer, and iii) each of the

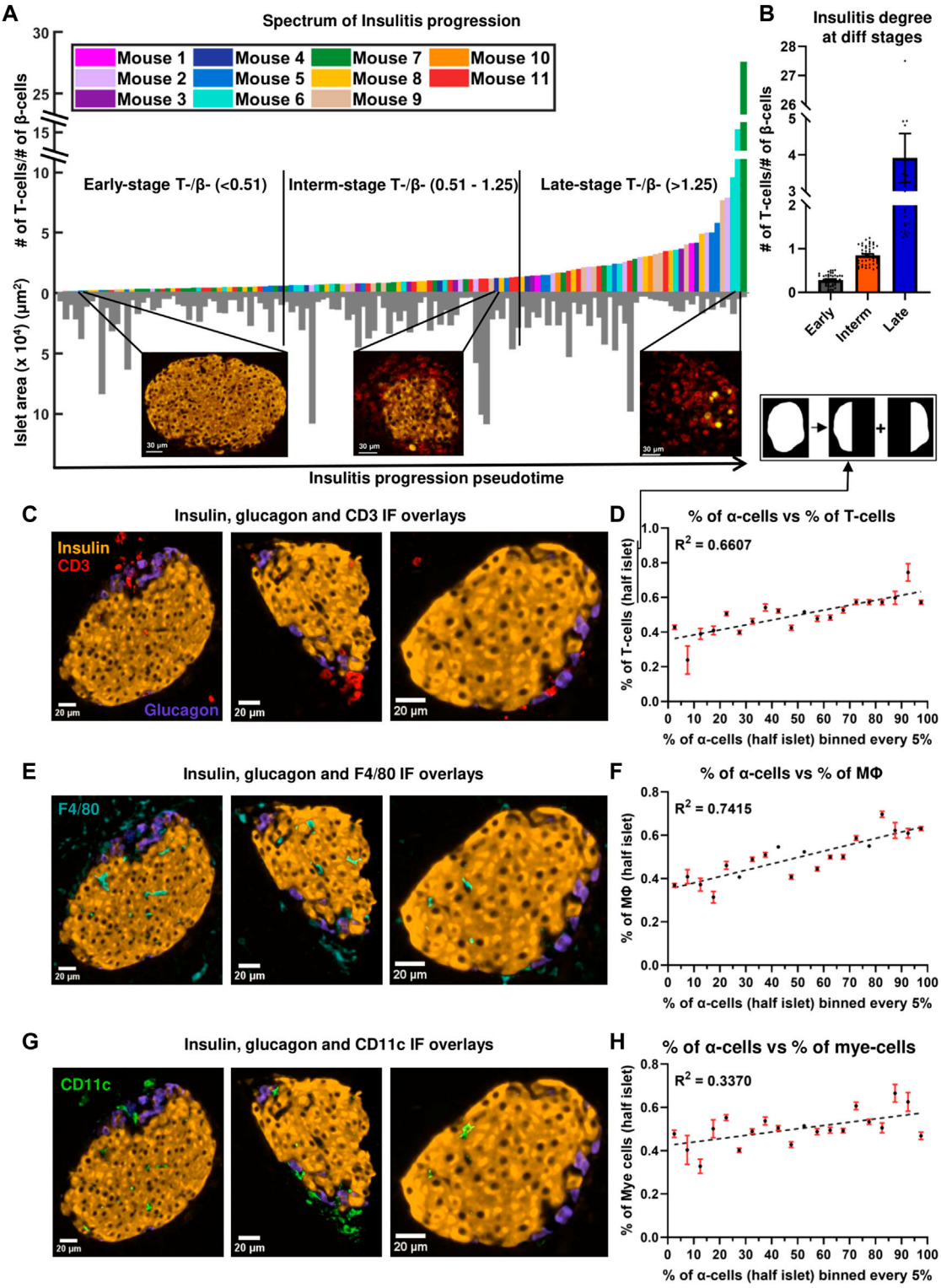

FIGURE 2
(A) Progression of insulitis in different islets, sorted using T/β cell ratios (pseudotime) (n = 134 islets from 11 mice). Orange and red colors in the immunofluorescent images correspond to insulin and CD3 stains. **(B)** Comparison of insulitis degrees of islets classified as early- (n = 44 islets), intermediate- (n = 46 islets), and late- (n = 44 islets) stage insulitis. **(C)** Immunofluorescence (IF) overlay of insulin (orange color), glucagon (purple color), and CD3 (red color) stains in three early-stage representative islets. **(D)** Relationship between the proportion of α-cells and the proportion of T-cells at a distance of at a distance of 20 μm from the islet rim in half islets (n = 134 islets from 11 mice). **(E)** IF overlay of insulin, glucagon, and F4/80 (cyan color) stains in three early-stage representative islets. **(F)** Relationship between the proportion of α-cells and the proportion of macrophages at a distance of at a distance of 20 μm from the islet rim in half islets (n = 134 islets from 11 mice). **(G)** IF overlay of insulin, glucagon, and CD11c (green color) stains in three early-stage representative islets. **(H)** Relationship between the proportion of α-cells and the proportion of myeloid cells at a distance of at a distance of
(*Continued*)

FIGURE 2 (Continued)
20 μm from the islet rim in half islets (n = 134 islets from 11 mice). Simple linear regression was used for statistical analysis in **(D,F)** and **(H)**. See Materials and Methods for a detailed description of the algorithm used to sort the islets and for how the proportion of α-cells and immune in half islets were determined.

immune cell types. β-cells linked to α cells were classified as "α-linked β-cells", and all other β-cells in the outer ring were classified as non-α-linked. The number of links between α-linked β-cells and immune cells was computed and compared to the number of links between non-α-linked β-cells and immune cells.

2.12 Determination of islet and immune cell proportions in islet halves

To assess whether immune cells preferentially infiltrate α-cell rich regions within an islet, we divided the islet mask into two-halves along a vertical or horizontal plane, as illustrated in Supplementary Figure S5A. We then calculated the number of islet cells (α- or β-) and immune cells (T-, macrophage, or myeloid cells) in each half, and then computed the proportion of each cell type within each section.

2.13 Network analysis to study inter-islet variations in islet size

To explore whether inter-islet size differences affect our observed trends, we categorized islets into three groups based on their cross-sectional area: small (0–7,000 μm^2), medium (7,000–20,000 μm^2), and large (>20,000 μm^2). Each group was then subdivided into early, intermediate, and late-stage insulitis based on their insulitis degrees. We then repeated various network analyses for each group, as shown in Supplementary Figures S10 and S12.

2.14 Statistical analysis

All statistical analysis was performed using GraphPad Prism (GraphPad, Boston, United States of America). Data was reported as ± SEM. The differences were considered to be statistically significant for $p < 0.05$. The tests used for evaluating statistical significance between results are mentioned in the figure captions.

3 Results

3.1 Network analysis can be successfully used as a tool to quantify cellular interactions.

We first sought to develop a metric that could quantify cellular interactions using the positions of various cells in an islet. Pancreatic tissue slices were stained for DAPI, insulin, glucagon, CD3, CD11c, and F4/80 and whole slide images were captured. As depicted in Figures 1A,B, an islet was first cropped from a whole slide image of the cross-section of a mouse's pancreas. Nuclei of cells were segmented for each of the channels and cross-referenced with the DAPI channel (Figures 1C–G). Euclidean distances were then computed between the cells, and finally, proximity-based networks were created using a suitable threshold as shown in Figure 1H (See Materials and Methods section for detailed description). We only considered the immune cells that were within 20 μm of the islet edge and all immune cells inside the islet. For network link assignment we tried different thresholds - 15, 20, and 25 μm, and saw the same trends (more or less pronounced based on the threshold) in our findings for each of them (Supplementary Figures S3, S8, S11). Therefore, we chose to use 20 μm as the threshold for network analysis. Finally, we observed modest colocalization between the immune cell markers (see Supplementary Figure S1 for more information), and, after image pre-processing, could ascertain that the CD3 channel correspond to T cells, CD11c to myeloid cells, and F4/80 to macrophages (Mϕ). We primarily sought to study the heterotypic interaction between two cell types, and we therefore generated networks for two types of cells at a time. We analyzed a total of 134 islets from 11 different mice (See Supplementary Figure S2 for more information on the age, glucose recordings, and the number of islets analyzed for each mouse).

As a first proof of concept, we compared the average number of connections (links), K_{avg} of α-cells in α–immune cell networks, and α–β cell network and observed the highest K_{avg} in α–β cell networks, which suggests that α-cells interact the most with β-cells, as expected (see Figure 1Q). Figures 1I–K represent the various α–immune networks for the islet shown in Figure 1B. Secondly, as a proof of concept, we compared the interactions between the different immune cell types cumulative for all islets by comparing the average links, also referenced through the text as *node degrees* or K_{avg} between T–myeloid cell networks, T-cell–macrophage networks and myeloid cell–macrophage networks (see Figure 1R). T - myeloid cell networks had a higher and significantly different K_{avg} compared to other immune cell pairs. These findings reinforce previous studies which state that T-cells and myeloid cells interact with each other during T1D (Calderon et al., 2011; Sandor et al., 2019; Jain et al., 2020), and support our use of the network analysis for assessment of cellular interaction. Lastly, to assess which immune cell *pairs* interact stronger with β-cells, we plotted the node degrees of various β–immune cell network pairs against each other and observed that β–myeloid cell network had the highest correlation coefficient (R^2) with the β–T cell network (see Figure 1S,T, and Supplementary Figure S3E). This suggests that the interaction of T-cells with β-cells correlates strongly with myeloid cell proximity and *vice versa*.

3.2 α-cell-rich regions of an islet are more infiltrated and characterized by non-random T- α and macrophage-α cell interactions.

To track the evolution of multicellular networks with peri-insulitis and insulitis progression, we computed the ratio of the number of T-cells and β-cells in each islet and sorted them in ascending order in Figure 2A (see detailed description in Materials and Methods). T/β cell ratios ranged from 0.0217 to 27.500. T/β cell ratios of islets of different pseudostages/stages of insulitis were compared in Figure 2B. The degree of infiltration in our early-, intermediate-, late-stage islets resembled the islets that were previously categorized as mild-, moderate-, and severe-insulitis (Miyazaki et al., 1985). As a proof of concept, we also plotted the T-cell density of the islets in the same spectrum obtained by sorting the ratios (pseudotime) and observed a similar exponential pattern as shown in Supplementary Figure S4A. The exponential patterns observed were also fit using log scales as shown in Supplementary Figures S4B and S4D. Next, we plotted the correlation between the number of β-cells and T-cells in an islet (Supplementary Figure S4E). By color-coding the stages, we observed distinct clusters with varying slopes, aligning within the predefined insulitis degree ranges for each stage.

Infiltration spectrum. As shown in the inserts in Figure 2A, islets at the beginning of the spectrum had sparse T-cells and intact β-cell mass (mostly peri-insulitis), islets at the center of the spectrum had an appreciable amount of intact β-cells and an increase in the number of T-cells (insulitis), and finally, islets at the end of the spectrum were destroyed, and had significant β-cell loss (destructive insulitis). In Supplementary Figure S4F we demonstrate the observed high heterogeneity in T-cell presence of different islets in the same mouse. The heterogeneity between mice in terms of T-cell presence has been previously observed (Johansson et al., 2003). On the other hand, the variability of islet inflammation in the *same* mouse has been known but often hindered by reporting the degree of insulitis in a mouse-averaged manner. Recently, categorizing insulitis progression (i.e., identifying a pseudo stage of the disease) in the islet-based manner has been used more widely (Carrero et al., 2013; Friedman et al., 2014; Lindsay et al., 2015; Katsarou et al., 2017; Damond et al., 2019). To eliminate the effect of external interactions on the polarity of immune cell infiltration, we have excluded the islets located at the edge of the tissue for subsequent analyses.

T cells and macrophages non-randomly interact with α-cells. We next sought to determine which immune cell type interacted the most with α-cells during the early stages of islet inflammation. We found that α–T cell networks had a higher number of links compared to α–macrophage and α–myeloid networks (p = 0.0067 and $p < 0.0001$) (see Figure 1Q). To determine whether the observed interactions between the immune cells and α-cells are due to chance, or if immune cells were drawn to α-cells, we generated random (or shuffled) networks where we fixed the positions of α-cells (same as experimentally observed) and randomly shuffled the positions of immune cells as shown in Figure 1I,M,N (see Materials and Methods and Supplementary Figure S6 for detailed description). After randomization, we observe a decrease in the number of α - immune cell links (Figure 3). An example of such non-uniform and non-random distribution of the immune cells is shown in the representative early-stage islet in Figures 3A, C, E. The upper region of the islet had more α-cells than the lower region. Perhaps as a result of that, the number of immune cells in the upper region of the islet was also higher. In the random (simulated) networks there was no significant difference of immune cell numbers in any regions of the islet.

α-immune interactions become random as the disease progresses. We then computed the average number of links of these random networks and compared them with the average number of links, K_{avg}, of the experimental networks in the early-, intermediate- and late-stages of the disease. In Figures 3B,D, we show that in the early stages of the disease, the K_{avg} of experimental α–T cell and α–macrophage networks was greater and more statistically significant than the corresponding random networks (p = 0.00380 and p = 0.0007). Experimental α–macrophage networks also exhibited more interactions than random networks in the intermediate stages (p = 0.0049). However, in the intermediate and later stage α–T cell networks the difference was not statistically significant and no significant differences were observed in the later stages of α–macrophage networks. These findings suggest that in the early stages of the disease the α - T as well as α - macrophage interactions, are not due to a chance. While we also observed an increase in the number of myeloid cells in α-cell rich regions of an islet (Figure 3E), the statistical significance was not observed between experimental and random α–myeloid cell networks (Figure 3F). Additionally, we observed similar results when we fixed the positions of immune cells and shuffled the positions of α-cells (see Supplementary Figure S7).

3.3 α-linked β-cells interact with T cells and macrophages stronger than non- α-linked.

In most of the islets classified to have an early-stage inflammation (examples are in Figures 2C, E, G) we observed that the α-cell-rich regions of the islet had more immune cells. This trend was diminished in the later stages of the disease. One can see more examples of this pattern in Supplementary Figure S9 where 7 out of 10 randomly picked early-stage islets exhibited this pattern of infiltration. We divided each islet into two regions using a vertical plane and observed a positive correlation between the percentage of α-cells and the percentage of immune cells in each region. (Figures 2D, F, H). We similarly noted a trend when employing a horizontal plane (Supplementary Figure S5B). Plotting the relationship between the percentage of β-cells and the percentage of immune cells revealed no correlation (see Supplementary Figures S5C and S5D), further indicating immune cells' preference for infiltrating α-cell rich regions of an islet. In order to detangle whether this effect is due to α-cells themselves, or α-linked β-cells, we then sought to quantify whether the β-cells closer to α-cells interact more with immune cells. To compensate for the fact that β-cells in the islet core have less chances to interact with immune cells at the early stages of insulitis, *i.e.,* to provide equal opportunity for both α-linked β-cells and non-α-linked β-cells to interact with immune cells near islet's surface, we considered only the peripheral (outer ring) β-cells (see Figures 4A,B) (see materials and methods for detailed description on how the outer ring was identified). Within the outer rings, we constructed networks between α-linked β-cells and immune cells,

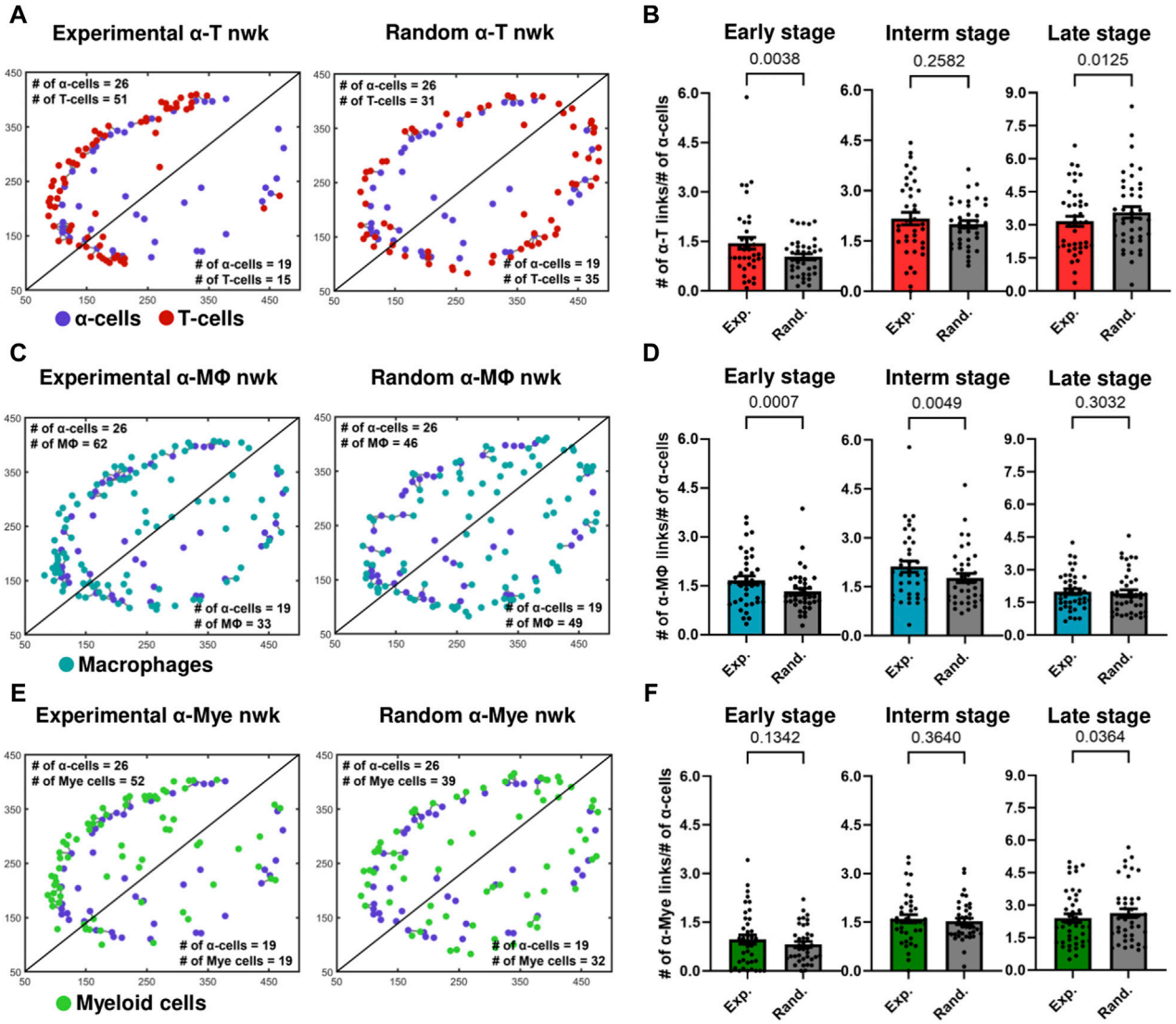

FIGURE 3
(A) Experimental and random α-cell–T-cell networks of a representative early-stage islet. **(B)** Comparison of K_{avg} of experimental and random α-cell–T-cell networks (nwks) in early- (n = 39 islets), intermediate- (interm) (n = 38 islets), and late- (n = 42 islets) stages using network analysis. **(C)** Experimental and random α-cell–macrophage (Mϕ) networks of a representative early-stage islet. **(D)** Comparison of K_{avg} of experimental and random α-cell–macrophage networks in early- (n = 39 islets), intermediate- (n = 38 islets), and late- (n = 42 islets) stages using network analysis. **(E)** Experimental and random α-cell–myeloid (mye) cell networks of a representative early-stage islet. **(F)** Comparison of K_{avg} of experimental and random α-cell–myeloid cell networks in early- (n = 39 islets), intermediate- (n = 38 islets), and late- (n = 42 islets) stages using network analysis. Paired parametric t-tests were used for statistical analysis in **(B,D)** and **(F)**. See Materials and Methods for detailed description of randomization and network analysis.

and non-α-linked β-cells and immune cells (see Figure 1L,O,P). We compared the K_{avg} of these networks at different stages of inflammation and found that the K_{avg} of α-linked β–T cell network was significantly greater than the K_{avg} of non-α-linked β–T cell networks in the early ($p < 0.0001$) stage (Figure 4D). Similarly, the K_{avg} of α-linked β-cell–macrophage networks was significantly greater than the K_{avg} of non-α-linked β-cell–macrophage networks in the early ($p = 0.0010$) and intermediate ($p = 0.0053$) stages (Figure 4F). However, in the later stages, the differences were no longer significant. No statistically significant trends were observed comparing the K_{avg} of α-linked β–myeloid cell and non-α-linked β–myeloid cell networks (Figure 4H). These observations suggest that the β-cells situated next to the α-cells (or interacting with α-cells) might interact more with the immune cells in the earlier stages of the disease. This is a novel finding not previously reported elsewhere.

4 Discussion

We successfully designed a workflow that could be used to quantify the cellular interactions using the proximity of cells in pancreatic islets during insulitis progression. In our dataset, we observed the presence of T-cells both in the periphery of the islet and inside the islet. Previously it was shown that the T-cells could traffic through the islet vasculature and extravasate into the islet

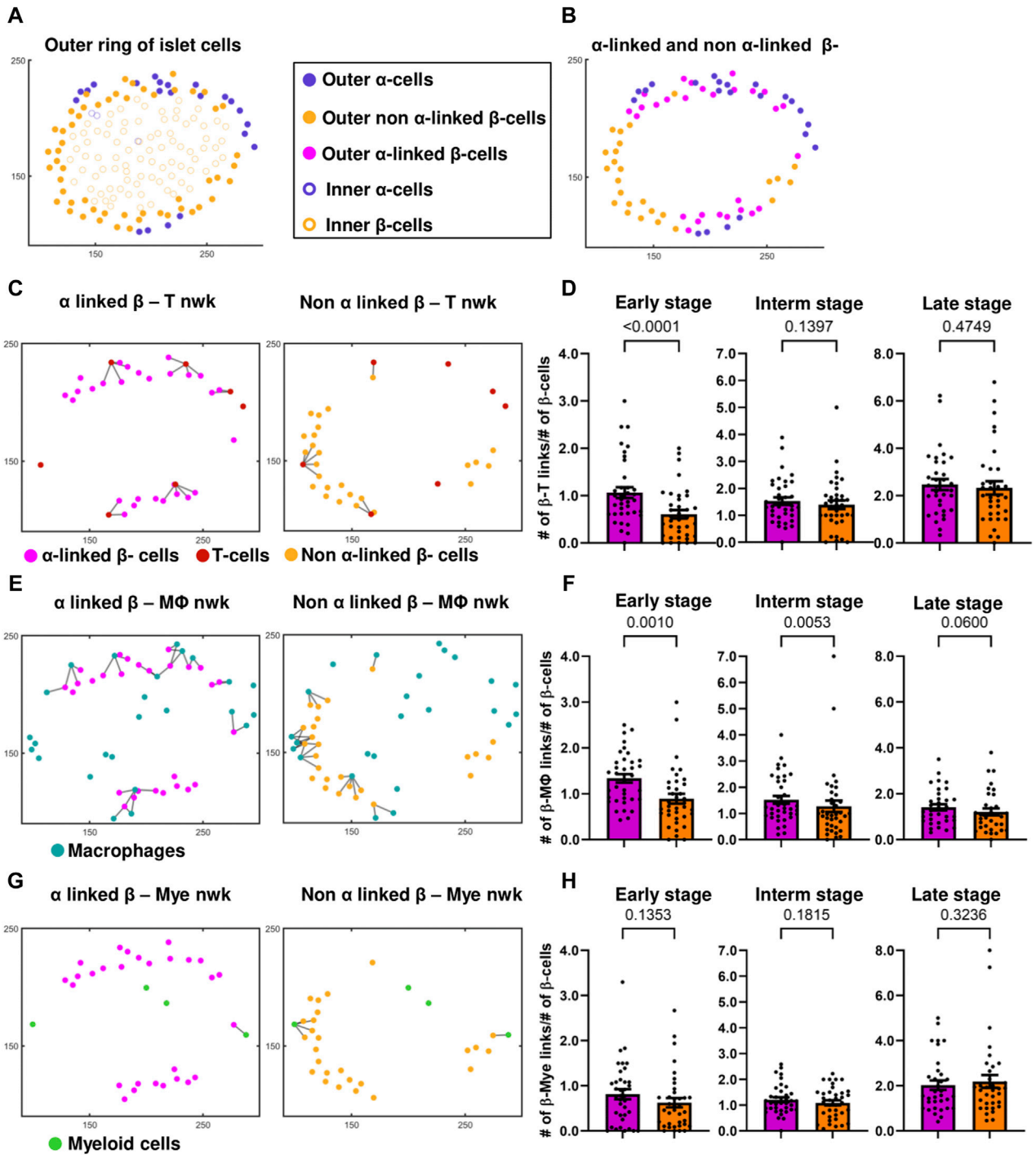

FIGURE 4
(A) Differentiation between the outer ring and inner core of islet cells, of a representative islet. **(B)** Identification of α-linked and non-α-linked β-cells in the outer ring of islet cells. **(C)** α-linked β-cell–and non-α-linked β-cell–T-cell networks (nwks) of a representative early-stage islet. **(D)** Comparison of K_{avg} of α-linked β-cell - and non-α-linked β-cell–T-cell networks in early (n = 37 islets), intermediate (interm) (n = 37 islets), and late (n = 34 islets) stages using network analysis. **(E)** α-linked β-cell–and non-α-linked β-cell–macrophage (Mϕ) networks of a representative early-stage islet. **(F)** Comparison of K_{avg} of α-linked β-cell and non-α-linked β-cell–macrophage networks in early (n = 37 islets), intermediate (n = 37 islets), and late (n = 34 islets) stages using network analysis. **(G)** α-linked β-cell–and non-α-linked β-cell–myeloid (mye) cell networks of a representative early-stage islet. **(H)** Comparison of K_{avg} of α-linked β-cell and non-α-linked β-cell–myeloid cell networks in early (n = 37 islets), intermediate (n = 37 islets), and late (n = 34 islets) stages using network analysis. Wilcoxon matched-pairs signed rank test was used for statistical analysis. See Materials and Methods for a detailed description of network analysis and on how the outer ring of islet cells was isolated.

(Sandor et al., 2019), explaining the presence of the T cells inside the islet. In the early stage, we observed the majority of the immune cells outside the islet (peri-insulitis). Our analysis showed β-cell associations with myeloid - T-cells pairs and macrophage - T-cell pairs. These observations can be rationalized by myeloid cells and macrophages being antigen-presenting cells, that release various chemokines responsible for T-cell recruitment and antigenic stimulation (Friedman et al., 2014; Lindsay et al., 2015; Sandor et al., 2019).

Why α-cell-rich areas of an islet have more leucocytes: In human islets, α-cells were reported to express more IL-1β, IL-6, and other non-classical MHC class 1 molecules than β-cells during T1D (Anquetil et al., 2017; Rajendran et al., 2020a; Benkahla et al., 2020; Rajendran et al., 2020b). Higher expression of pro-inflammatory cytokines, could increase inflammation in the α-cell-rich regions of the islet, and potentially explain why immune cells are drawn to these regions in the early stages of disease. In 12- to 21-week-old NOD mice, α-cells were reported to express more CXCL10 (a chemokine recognized by the CXCR3 receptor of T-cells) (Nigi et al., 2020). Glucagon–CXCL10 colocalization, was greater than insulin–CXCL10 colocalization in new-onset diabetic NOD mice, and further increases on diabetes onset (Nigi et al., 2020). Increased expression of CXCL10 by α-cells could also potentially explain the presence of more T-cells and macrophages in the α-cell rich regions of an islet (Figures 2C 2D 2E,F). Previous studies have indicated that the increased expression of CXCL10 increases T-cell and macrophage infiltration in the islet and that diabetogenic T-cells migrate to sites containing higher levels of CXCL10 (Christen et al., 2004; Tanaka et al., 2009; Roep et al., 2010). It is important to note that while α-cells interact with T-cells and macrophages in the early stages, the α-cells still remain alive until very advanced stages of diabetes (Bru-Tari et al., 2019). Additionally, in the later stages of islet inflammation, we do not notice specific interactions between the α-cells and immune cells (Figures 3B 3D,F), possibly due to an increase in myeloid cell infiltration, myeloid cell–T cell interactions, and an overall increase in CXCL10 expression throughout the islet (Shigihara et al., 2006; Sandor et al., 2019).

Why α-linked β-cells have more leucocyte interactions: Firstly, β-cell proximity to α-cells increases their exposure to glucagon and GLP1, which is sensed via GLP1-R on the surface of the β-cells and increases cyclic AMP and insulin production (Moens et al., 1998; Marchetti et al., 2012). Our discovery of T-cells and macrophages' non-random interaction with α-linked β-cells may be rationalized by higher amounts of insulin produced by α-linked β-cells. This effect is more pronounced in larger-sized islets (see Supplementary Figure S12), as there are fewer β-cells in smaller-sized islets, leading to a higher proportion of β-cells being influenced by the glucagon released by α-cells. Secondly, in humans and rodents, β-cells exhibit a distinct biphasic insulin response to glucose stimulation (Curry et al., 1968; Porte and Pupo, 1969; Nunemaker et al., 2006). There is a marked loss in the first phase of insulin secretion in individuals with pre-diabetes and with T1D (Brunzell et al., 1976). We previously showed that, first responder β-cells are a subpopulation of β-cells that drive this first phase of islet's response to glucose, and that ablation of these first responder β-cells leads to a loss in first phase response (Kravets et al., 2022). First responder β-cells are also located closer to α-cells (Kravets et al., 2023), which combined with our finding in this work, suggests that it is likely that first responder β-cells are affected sooner than other β-cells during insulitis. This, in turn, means that loss of the first phase of insulin secretion may be due to immune-mediated destruction of the first responder β-cells by the T cells.

The main limitations of our study are as follows. Our work was done on the fixed tissue, and the networks were constructed based on the proximity of the immune cells to endocrine cells. It would be more beneficial to study dynamic interactions in live tissue, which is relatively difficult to do due to the scarcity and fragility of the live human tissue samples. Additionally, we studied cellular interactions in a 2D tissue, studying cellular interactions in a 3D microenvironment with the addition of the markers for vasculature will provide more insights into the changes in islet architecture with disease progression. Moreover, the $CD3^+$ T-cells in our study encompass both helper and cytotoxic T-cells, it would be more beneficial to study the interactions between islet cells and each subpopulation of T-cells separately, as the two types of T cells have different roles in the pathogenesis of T1D. Finally, the network analysis technique employed in this study assumes that cells are interacting based on the proximities of the cells, however studying functional networks, *in vitro* and *in vivo* will provide more insights. Future studies can focus on the role of α-cells in the early stages of T1D, and what properties of α-cells, and α-linked β-cells make them more susceptible to immune attack.

5 Conclusion

Overall, the findings indicate dynamic changes in endocrine-immune cell interactions during the progression of insulitis and shine new light on the α-linked β-cells, or α-cells as potential primary targets. Non-random T-cell and macrophage interactions with α-cells, the polarization of peri-insulitis and insulitis patterns towards α-rich regions of the islet early in disease progression, and most importantly, significant prevalence of α-linked β-cell interactions with immune cells suggests that these cells will be lost first in T1D.

Data availability statement

The MATLAB scripts used to implement network analysis to quantify contact-based cellular interactions can be accessed at https://doi.org/10.5281/zenodo.11287007, and the whole slide images of the mouse pancreatic cross sections stained with the antibodies used in our study are available at https://doi.org/10.6019/S-BIAD1184. For further inquiries or additional data requests, please contact the corresponding author.

Ethics statement

The animal study was approved by Institutional Animal Care and Use Committee at the University of Colorado Anschutz Medical Campus. The study was conducted in accordance with the local legislation and institutional requirements.

Author contributions

NB: Formal Analysis, Investigation, Software, Visualization, Writing–original draft. JW: Data curation, Investigation, Methodology, Writing–review and editing. LP: Formal analysis, Software, Writing–review and editing. RF: Data curation, Funding acquisition, Methodology, Project administration, Resources, Supervision, Writing–review and editing. VK: Conceptualization, Funding acquisition, Methodology, Project administration, Resources, Software, Supervision, Validation, Visualization, Writing–review and editing.

Funding

The author(s) declare that financial support was received for the research, authorship, and/or publication of this article. This work was funded by Burroughs Wellcome Fund CASI award (Project 25B1756) and Human Islets Research Network subaward (HIRN, RRID:SCR_014393; UC24 DK104162) to VK; R01-DK111733 to RF; and the Colorado Diabetes Research Center (P30DK11607).

Acknowledgments

We are grateful for constructive suggestions from Marko Gosak who provided his feedback at the early stage of this project, Kimberly Jordan and Angela Minic in the Human Immune Shared Resource, and Brittany Basta for support of our animal colony.

Conflict of interest

The authors declare that the research was conducted in the absence of any commercial or financial relationships that could be construed as a potential conflict of interest.

Publisher's note

Supplementary material

The Supplementary Material for this article can be found online at: https://www.frontiersin.org/articles/10.3389/fnetp.2024.1393397/full#supplementary-material

References

Anderson, M. S., and Bluestone, J. A. (2005). The NOD mouse: a model of immune dysregulation. *Annu. Rev. Immunol.* 23, 447–485. doi:10.1146/annurev.immunol.23.021704.115643

Anquetil, F., Sabouri, S., Thivolet, C., Rodriguez-Calvo, T., Zapardiel-Gonzalo, J., Amirian, N., et al. (2017). Alpha cells, the main source of IL-1β in human pancreas. *J. Autoimmun.* 81, 68–73. doi:10.1016/j.jaut.2017.03.006

Barabási, A.-L., Gulbahce, N., and Loscalzo, J. (2011). Network medicine: a network-based approach to human disease. *Nat. Rev. Genet.* 12 (1), 56–68. doi:10.1038/nrg2918

Barabási, A.-L., and Oltvai, Z. N. (2004). Network biology: understanding the cell's functional organization. *Nat. Rev. Genet.* 5 (2), 101–113. doi:10.1038/nrg1272

Benkahla, M. A., Sabouri, S., Kiosses, W. B., Rajendran, S., Quesada-Masachs, E., and von Herrath, M. (2020). Overexpression of HLA class I predominantly on alpha cell in at risk individuals for type 1 diabetes. *bioRxiv*. doi:10.1101/2020.07.13.201079

Brunzell, J. D., Robertson, R. P., Lerner, R. L., Hazzard, W. R., Ensinck, J. W., Bierman, E. L., et al. (1976). Relationships between fasting plasma glucose levels and insulin secretion during intravenous glucose tolerance tests. *J. Clin. Endocrinol. Metab.* 42 (2), 222–229. doi:10.1210/jcem-42-2-222

Bru-Tari, E., Cobo-Vuilleumier, N., Alonso-Magdalena, P., Dos Santos, R. S., Marroqui, L., Nadal, A., et al. (2019). Pancreatic alpha-cell mass in the early-onset and advanced stage of a mouse model of experimental autoimmune diabetes. *Sci. Rep.* 9 (1), 9515. doi:10.1038/s41598-019-45853-1

Bullmore, E., and Sporns, O. (2009). Complex brain networks: graph theoretical analysis of structural and functional systems. *Nat. Rev. Neurosci.* 10 (3), 186–198. doi:10.1038/nrn2575

Burrack, A. L., Martinov, T., and Fife, B. T. (2017). T cell-mediated beta cell destruction: autoimmunity and alloimmunity in the context of type 1 diabetes. *Front. Endocrinol. (Lausanne)* 8, 343. doi:10.3389/fendo.2017.00343

Caicedo, A. (2013). Paracrine and autocrine interactions in the human islet: more than meets the eye. *Semin. Cell Dev. Biol.* 24 (1), 11–21. doi:10.1016/j.semcdb.2012.09.007

Calderon, B., Carrero, J. A., Miller, M. J., and Unanue, E. R. (2011). Cellular and molecular events in the localization of diabetogenic T cells to islets of Langerhans. *Proc. Natl. Acad. Sci. U. S. A.* 108 (4), 1561–1566. doi:10.1073/pnas.1018973108

Carrero, J. A., Calderon, B., Towfic, F., Artyomov, M. N., and Unanue, E. R. (2013). Defining the transcriptional and cellular landscape of type 1 diabetes in the NOD mouse. *PLoS One* 8 (3), e59701. doi:10.1371/journal.pone.0059701

Chen, D., Thayer, T. C., Wen, L., and Wong, F. S. (2020). "Mouse models of autoimmune diabetes: the nonobese diabetic (NOD) mouse," in *Methods in molecular Biology* (New York, NY: Springer US), 87–92.

Christen, U., Benke, D., Wolfe, T., Rodrigo, E., Rhode, A., Hughes, A. C., et al. (2004). Cure of prediabetic mice by viral infections involves lymphocyte recruitment along an IP-10 gradient. *J. Clin. Invest.* 113 (1), 74–84. doi:10.1172/JCI17005

Cnop, M., Welsh, N., Jonas, J. C., Jorns, A., Lenzen, S., and Eizirik, D. L. (2005). Mechanisms of pancreatic beta-cell death in type 1 and type 2 diabetes: many differences, few similarities. *Diabetes* 54 (Suppl. 2), S97–S107. doi:10.2337/diabetes.54.suppl_2.s97

Coppieters, K. T., Dotta, F., Amirian, N., Campbell, P. D., Kay, T. W., Atkinson, M. A., et al. (2012). Demonstration of islet-autoreactive CD8 T cells in insulitic lesions from recent onset and long-term type 1 diabetes patients. *J. Exp. Med.* 209 (1), 51–60. doi:10.1084/jem.20111187

Costes, S. V., Daelemans, D., Cho, E. H., Dobbin, Z., Pavlakis, G., and Lockett, S. (2004). Automatic and quantitative measurement of protein-protein colocalization in live cells. *Biophys. J.* 86 (6), 3993–4003. doi:10.1529/biophysj.103.038422

Curry, D. L., Bennett, L. L., and Grodsky, G. M. (1968). Dynamics of insulin secretion by the perfused rat pancreas. *Endocrinology* 83 (3), 572–584. doi:10.1210/endo-83-3-572

Damond, N., Engler, S., Zanotelli, V. R. T., Schapiro, D., Wasserfall, C. H., Kusmartseva, I., et al. (2019). A map of human type 1 diabetes progression by imaging mass cytometry. *Cell Metab.* 29 (3), 755–768. doi:10.1016/j.cmet.2018.11.014

Daniels, M. A., and Jameson, S. C. (2000). Critical role for CD8 in T cell receptor binding and activation by peptide/major histocompatibility complex multimers. *J. Exp. Med.* 191 (2), 335–346. doi:10.1084/jem.191.2.335

Dudek, N. L., Thomas, H. E., Mariana, L., Sutherland, R. M., Allison, J., Estella, E., et al. (2006). Cytotoxic T-cells from T-cell receptor transgenic NOD8.3 mice destroy beta-cells via the perforin and Fas pathways. *Diabetes* 55 (9), 2412–2418. doi:10.2337/db06-0109

Friedl, P., and Gunzer, M. (2001). Interaction of T cells with APCs: the serial encounter model. *Trends Immunol.* 22 (4), 187–191. doi:10.1016/s1471-4906(01)01869-5

Friedman, R. S., Lindsay, R. S., Lilly, J. K., Nguyen, V., Sorensen, C. M., Jacobelli, J., et al. (2014). An evolving autoimmune microenvironment regulates the quality of effector T cell restimulation and function. *Proc. Natl. Acad. Sci. U. S. A.* 111 (25), 9223–9228. doi:10.1073/pnas.1322193111

Gosak, M., Milojevic, M., Duh, M., Skok, K., and Perc, M. (2022). Networks behind the morphology and structural design of living systems. *Phys. Life Rev.* 41, 1–21. doi:10.1016/j.plrev.2022.03.001

Hoang, D.-T., Matsunari, H., Nagaya, M., Nagashima, H., Millis, J. M., Witkowski, P., et al. (2014). A conserved rule for pancreatic islet organization. *PLoS One* 9 (10), e110384. doi:10.1371/journal.pone.0110384

Jain, A., Irizarry-Caro, R. A., McDaniel, M. M., Chawla, A. S., Carroll, K. R., Overcast, G. R., et al. (2020). T cells instruct myeloid cells to produce inflammasome-independent IL-1β and cause autoimmunity. *Nat. Immunol.* 21 (1), 65–74. doi:10.1038/s41590-019-0559-y

Jeong, H., Tombor, B., Albert, R., Oltvai, Z. N., and Barabási, A. L. (2000). The large-scale organization of metabolic networks. *Nature* 407 (6804), 651–654. doi:10.1038/35036627

Johansson, A. C. M., Lindqvist, A. K. B., Johannesson, M., and Holmdahl, R. (2003). Genetic heterogeneity of autoimmune disorders in the nonobese diabetic mouse. *Scand. J. Immunol.* 57 (3), 203–213. doi:10.1046/j.1365-3083.2003.01235.x

Johnston, N. R., Mitchell, R. K., Haythorne, E., Pessoa, M. P., Semplici, F., Ferrer, J., et al. (2016). Beta cell hubs dictate pancreatic islet responses to glucose. *Cell Metab.* 24 (3), 389–401. doi:10.1016/j.cmet.2016.06.020

Katsarou, A., Gudbjörnsdottir, S., Rawshani, A., Dabelea, D., Bonifacio, E., Anderson, B. J., et al. (2017). Type 1 diabetes mellitus. *Nat. Rev. Dis. Prim.* 3 (1), 17016. doi:10.1038/nrdp.2017.16

Kikutani, H., and Makino, S. (1992). The Murine autoimmune diabetes model: NOD and related strains. *Adv. Immunol.* 51, 285–322. doi:10.1016/s0065-2776(08)60490-3

Kravets, V., Dwulet, J. M., Schleicher, W. E., Hodson, D. J., Davis, A. M., Pyle, L., et al. (2022). Functional architecture of pancreatic islets identifies a population of first responder cells that drive the first-phase calcium response. *PLoS Biol.* 20 (9), e3001761. doi:10.1371/journal.pbio.3001761

Kravets, V., Levitt, C. H., and Benninger, R. K. (2023). 195-OR: to which degree do alpha cells shape the role of the beta cells first responders? *Diabetes* 72 (Suppl. ment_1). doi:10.2337/db23-195-OR

Lindsay, R. S., Corbin, K., Mahne, A., Levitt, B. E., Gebert, M. J., Wigton, E. J., et al. (2015). Antigen recognition in the islets changes with progression of autoimmune islet infiltration. *J. Immunol.* 194 (2), 522–530. doi:10.4049/jimmunol.1400626

Manders, E. M. M., Verbeek, F. J., and Aten, J. A. (1993). Measurement of co-localization of objects in dual-colour confocal images. *J. Microsc.* 169 (3), 375–382. doi:10.1111/j.1365-2818.1993.tb03313.x

Marchetti, P., Lupi, R., Bugliani, M., Kirkpatrick, C. L., Sebastiani, G., Grieco, F. A., et al. (2012). A local glucagon-like peptide 1 (GLP-1) system in human pancreatic islets. *Diabetologia* 55 (12), 3262–3272. doi:10.1007/s00125-012-2716-9

Mariuzza, R. A., Agnihotri, P., and Orban, J. (2020). The structural basis of T-cell receptor (TCR) activation: an enduring enigma. *J. Biol. Chem.* 295 (4), 914–925. doi:10.1074/jbc.REV119.009411

Miyazaki, A., Hanafusa, T., Yamada, K., Miyagawa, J., Fujino-Kurihara, H., Nakajima, H., et al. (1985). Predominance of T lymphocytes in pancreatic islets and spleen of pre-diabetic non-obese diabetic (NOD) mice: a longitudinal study. *Clin. Exp. Immunol.* 60 (3), 622–630.

Moens, K., Flamez, D., Van Schravendijk, C., Ling, Z., Pipeleers, D., and Schuit, F. (1998). Dual glucagon recognition by pancreatic beta-cells via glucagon and glucagon-like peptide 1 receptors. *Diabetes* 47 (1), 66–72. doi:10.2337/diab.47.1.66

Morgan, N. G., Leete, P., Foulis, A. K., and Richardson, S. J. (2014). Islet inflammation in human type 1 diabetes mellitus. *IUBMB Life* 66 (11), 723–734. doi:10.1002/iub.1330

Nigi, L., Brusco, N., Grieco, G. E., Licata, G., Krogvold, L., Marselli, L., et al. (2020). Pancreatic alpha-cells contribute together with beta-cells to CXCL10 expression in type 1 Diabetes. *Front. Endocrinol. (Lausanne)* 11, 630. doi:10.3389/fendo.2020.00630

Nunemaker, C. S., Wasserman, D. H., McGuinness, O. P., Sweet, I. R., Teague, J. C., and Satin, L. S. (2006). Insulin secretion in the conscious mouse is biphasic and pulsatile. *Am. J. Physiol. Endocrinol. Metab.* 290 (3), E523–E529. doi:10.1152/ajpendo.00392.2005

Porte, D., and Pupo, A. A. (1969). Insulin responses to glucose: evidence for a two pool system in man. *J. Clin. Invest.* 48 (12), 2309–2319. doi:10.1172/JCI106197

Rajendran, S., Anquetil, F., Quesada-Masachs, E., Graef, M., Gonzalez, N., McArdle, S., et al. (2020a). IL-6 is present in beta and alpha cells in human pancreatic islets: expression is reduced in subjects with type 1 diabetes. *Clin. Immunol.* 211 (108320), 108320. doi:10.1016/j.clim.2019.108320

Rajendran, S., Graef, M., Chu, T., and von Herrath, M. (2020b). IL-4R is expressed on alpha and beta cells of human pancreata. *Clin. Immunol.* 214 (108394), 108394. doi:10.1016/j.clim.2020.108394

Rodriguez-Calvo, T., Suwandi, J. S., Amirian, N., Zapardiel-Gonzalo, J., Anquetil, F., Sabouri, S., et al. (2015). Heterogeneity and lobularity of pancreatic pathology in type 1 diabetes during the prediabetic phase. *J. Histochem. Cytochem.* 63 (8), 626–636. doi:10.1369/0022155415576543

Roep, B. O., Kleijwegt, F. S., Van Halteren, A. G. S., Bonato, V., Boggi, U., Vendrame, F., et al. (2010). Islet inflammation and CXCL10 in recent-onset type 1 diabetes. *Clin. Exp. Immunol.* 159 (3), 338–343. doi:10.1111/j.1365-2249.2009.04087.x

Sandor, A. M., Lindsay, R. S., Dyjack, N., Whitesell, J. C., Rios, C., Bradley, B. J., et al. (2019). CD11c+ cells are gatekeepers for lymphocyte trafficking to infiltrated islets during type 1 diabetes. *Front. Immunol.* 10, 99. doi:10.3389/fimmu.2019.00099

Schindelin, J., Arganda-Carreras, I., Frise, E., Kaynig, V., Longair, M., Pietzsch, T., et al. (2012). Fiji: an open-source platform for biological-image analysis. *Nat. Methods* 9 (7), 676–682. doi:10.1038/nmeth.2019

Schlitt, T., and Brazma, A. (2007). Current approaches to gene regulatory network modelling. *BMC Bioinforma.* 8 (6), S9. doi:10.1186/1471-2105-8-S6-S9

Shigihara, T., Oikawa, Y., Kanazawa, Y., Okubo, Y., Narumi, S., Saruta, T., et al. (2006). Significance of serum CXCL10/IP-10 level in type 1 diabetes. *J. Autoimmun.* 26 (1), 66–71. doi:10.1016/j.jaut.2005.09.027

Stožer, A., Gosak, M., Dolenšek, J., Perc, M., Marhl, M., Rupnik, M. S., et al. (2013). Functional connectivity in islets of Langerhans from mouse pancreas tissue slices. *PLoS Comput. Biol.* 9 (2), e1002923. doi:10.1371/journal.pcbi.1002923

Stožer, A., Šterk, M., Paradiž Leitgeb, E., Markovič, R., Skelin Klemen, M., Ellis, C. E., et al. (2022). From isles of königsberg to islets of Langerhans: examining the function of the endocrine pancreas through network science. *Front. Endocrinol. (Lausanne)* 13, 922640. doi:10.3389/fendo.2022.922640

Tanaka, S., Nishida, Y., Aida, K., Maruyama, T., Shimada, A., Suzuki, M., et al. (2009). Enterovirus infection, CXC chemokine ligand 10 (CXCL10), and CXCR3 circuit: a mechanism of accelerated beta-cell failure in fulminant type 1 diabetes. *Diabetes* 58 (10), 2285–2291. doi:10.2337/db09-0091

Tran Thi Nhu, H., Arrojo, E., Drigo, R., Berggren, P.-O., and Boudier, T. (2017). A novel toolbox to investigate tissue spatial organization applied to the study of the islets of Langerhans. *Sci. Rep.* 7 (1), 44261. doi:10.1038/srep44261

Vomund, A. N., Zinselmeyer, B. H., Hughes, J., Calderon, B., Valderrama, C., Ferris, S. T., et al. (2015). Beta cells transfer vesicles containing insulin to phagocytes for presentation to T cells. *Proc. Natl. Acad. Sci. U. S. A.* 112 (40), E5496–E5502. doi:10.1073/pnas.1515954112